

Myocardial tissue oxygenation estimated with calibrated diffuse reflectance spectroscopy during coronary artery bypass grafting

Erik Häggblad
Tobias Lindbergh
M. G. Daniel Karlsson

Linköping University
Department of Biomedical Engineering
Linköping Biomedical Optics Group
Linköping, Sweden

Henrik Casimir-Ahn

University Hospital
Linköping Heart Center
Linköping, Sweden

E. Göran Salerud

Tomas Strömberg
Linköping University
Department of Biomedical Engineering
Linköping Biomedical Optics Group
Linköping, Sweden

Abstract. We present a study using a method able to assess tissue oxygenation, taking into account the absorption and the level of scattering in myocardial tissue using a calibrated fiber optic probe. With this method, interindividual comparisons of oxygenation can be made despite varying tissue optical properties during coronary artery bypass grafting (CABG). During CABG, there are needs for methods allowing continuous monitoring and prediction of the metabolism in the myocardial tissue. 14 patients undergoing CABG are investigated for tissue oxygenation during different surgical phases using a handheld fiber optic spectroscopic probe with a source-detector distance of less than 1 mm. The probe is calibrated using a light transport model, relating the absorption and reduced scattering coefficients (μ_a and μ'_s) to the measured spectra. By solving the inverse problem, absolute measures of tissue oxygenation are evaluated by the sum of oxygenized hemoglobin and myoglobin. Agreement between the model and measurements is obtained with an average correlation coefficient R^2 of 0.96. Oxygenation is found to be significantly elevated after aorta cross-clamping and cardioplegic infusion, as well as after reperfusion, compared to a baseline ($p < 0.05$). Tissue oxygenation decreases during cardiac arrest and increases after reperfusion. © 2008 Society of Photo-Optical Instrumentation Engineers. [DOI: 10.1117/1.2976433]

Keywords: diffuse reflectance spectroscopy; oxygenation; myocardium; tissue; coronary artery bypass grafting.

Paper 07367R received Sep. 6, 2007; revised manuscript received Feb. 8, 2008; accepted for publication May 24, 2008; published online Sep. 15, 2008.

1 Introduction

The surgery technique, coronary artery bypass grafting (CABG), is carried out on more than 800,000 patients annually.¹ During the CABG procedure, the heart is exposed to both mechanical and physiological workloads, where the interaction of myocardial circulation and metabolic needs will affect tissue oxygenation. It is essential that heart metabolism is minimal when coronary circulation is abolished during the transfer of systemic circulation from the heart to the extracorporeal circulation system (ECC). Furthermore, during the re-establishment of coronary circulation, it is important that the blood flow and oxygen supply meet the requirements of the increased tissue metabolism. Consequently, there are needs for methods allowing continuous monitoring and prediction of the metabolism and perfusion parameters during surgery and postoperatively. Local perfusion in myocardial tissue micro-circulation can be measured with ECG-triggered laser Doppler flowmetry.² However, the estimation of perfusion is affected by motion artifacts when heart movement is irregular. Intramyocardial partial oxygen pressure, an indicator of oxygen supply and demand, has been measured using a polaro-

graphic technique.³ This method is based on diffusion equilibrium across a membrane, which introduces a time constant and may cause protein adhesion. Diffuse reflectance spectroscopy (DRS), which has previously been used in other studies on the heart,⁴⁻⁷ utilizes the characteristic spectral absorption of the oxygen-dependent chromophores, hemoglobin, and myoglobin, as well as the cytochromes. These chromophores depict the oxygen transport from blood to myoglobin in the myocardial tissue and the last step in the electron transfer chain during mitochondrial respiration. However, myoglobin and hemoglobin spectra are similar, so their sum is often assessed,⁸ although their relative importance to oxygen transport can be estimated by carefully studying the spectral peaks and troughs in the 540 to 580-nm band.⁵ Cytochrome aa3, being the last step in the electron transfer chain, is often assessed as relative changes in its reduction-oxidation state by determining the absorption around 830 nm.⁸ In our study, we used a calibrated DRS fiber optic surface probe for spectral determination of the absorption (μ_a) and the reduced scattering coefficients (μ'_s) in the myocardial tissue reflecting changes in myocardial metabolism. The technique has previously been proposed by Jacques, Bargo, and Engelking.⁹ Recorded spectra are normalized using a custom-built solid

Address all correspondence to Erik Häggblad, Dept. of Biomedical Engineering, Linköping Universitet, Campus US, Linköping, SE 58223, Sweden; Tel: +46 13 222 466; Fax: +46 13 10 19 02; E-mail: eriha@imt.liu.se

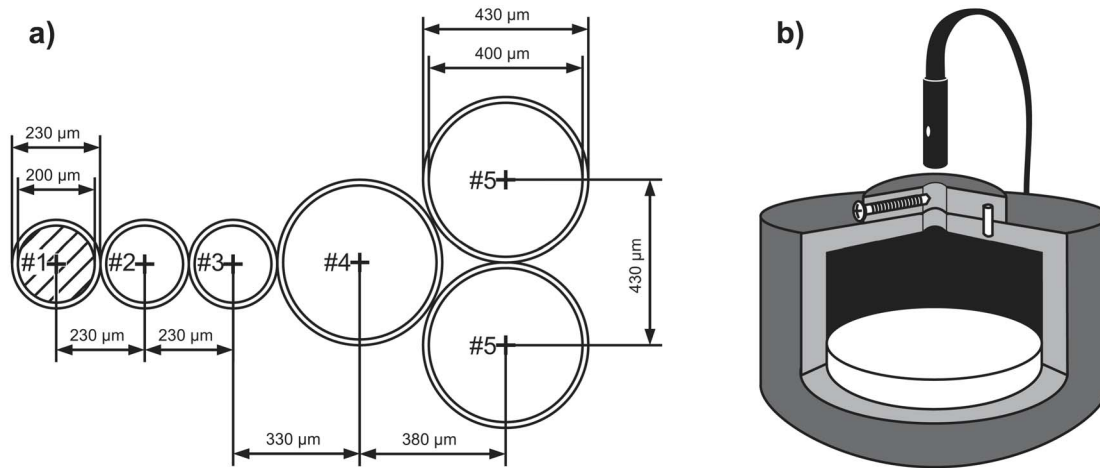


Fig. 1 (a) The probe design indicating the different fiber distances and the fiber sizes. A hatched fiber indicates an emitting fiber and numbers indicate spectroscopic channels used for each fiber separation distance. (b) A cut-out view of the solid phantom used for day-to-day calibration of light intensity and color. The enclosing housing is of black plastic and the illuminated area (white) is of polyacetal plastic with a medium grained surface, ensuring diffusively reflected light.

phantom and are white-corrected using a white reference. Calibration is performed using a set of liquid optical phantoms with known optical properties covering those present in the tissue of interest. Thereafter, the light transport model for absorption (μ_a) and reduced scattering (μ'_s) is fitted to the recorded spectra. The μ_a in the model is a linear combination of the chosen chromophores and can consequently be fractionally decomposed.

The aim of this study was to develop a calibrated DRS system for assessment of myocardial tissue oxygenation during CABG.

2 Material and Methods

2.1 Subjects

14 patients (10 males, 4 females), age 54 to 81, were enrolled after giving informed consent. The chosen patients underwent CABG and the number of grafts sutured varied between three and six. This study was approved by the Regional Ethical Review Board for Medical Research in Linköping (number LiU486/03-14).

2.2 Surgical Procedure

Following normal clinical routines, patients were anesthetized and intubated before a midline sternotomy was performed to expose the heart. Simultaneously, the left internal mammary artery (LIMA) and the saphenous vein were harvested to be used as bypass grafts. As a preparation, the heart-lung machine was primed with 1.5-L cold crystalloid cardioplegic solution and connected to the patient after full heparinization. Extracorporeal circulation (ECC) was established, and at full flow, the ascending aorta was cross-clamped. Cardioplegic solution was immediately introduced into the coronary arteries via a small cannula at the aortic root. This infusion of potassium causes a rapid washout of blood in the coronary artery circulation system and a subsequent cardiac arrest. The time from aortic cross-clamping and cardioplegic infusion until cardiac arrest varied between 30 to 50 s, as estimated by the

surgeon. Thereafter the required numbers of anastomoses were performed. Cardioplegic solution was administered every 20 min to maintain low myocardial metabolism and temperature throughout the surgical procedure.

Myocardial reperfusion is initiated by partial blood-filling of the heart, and subsequent removal of the aortic cross-clamp. Simultaneously, additional clamps used to prevent blood from flowing into the coronary system through the sutured grafts were removed. In most cases, both the proximal and distal anastomoses were performed before releasing the aortic cross-clamp. However, in two patients (cases 1 and 2), the aortic cross-clamp was released before performing the proximal anastomoses; alternatively, only a small segment of the ascending aorta wall was clamped to enable suturing of the proximal part of the grafts. Subsequently, the partial clamping of the aorta was released, and blood perfusion established in the area was supported by each specific graft. This procedure of partial clamping reduces the time of no blood flow to the myocardial tissue, since blood is allowed to enter the heart through partial blood-filling via the ECC while performing the proximal anastomoses.

After achieving a stable heart condition for the patient, the ECC was gradually phased out until removal, and finally the chest was closed.

2.3 Equipment

During the measurements we used a multichannel spectrometer (AvaSpec 2048-5-RM, Avantes BV, The Netherlands) operating in the visible wavelength region (400 to 900 nm, grating VB 600 lines/mm). The emitting light source was a broadband tungsten halogen lamp (HL-2000, Ocean Optics Incorporated). The custom-built fiber optic surface probe comprised one bifurcated illuminating fiber ($\varnothing=230 \mu\text{m}$) and a fiber design that enabled four different detection distances of the probe (230, 460, 790, and 1170 μm) shown in Fig. 1(a). An increasing emitting-receiving fiber distance enables a deeper sampling depth and hence gives a possibility to study different volumes of the tissue. To account for varia-

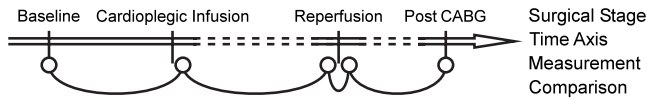


Fig. 2 Calibrated diffuse reflectance measurements (circles) in relation to the surgical procedure. The comparisons evaluated in the data analysis are indicated by the curves joining the circles.

tions in detected light intensity, we have used a custom-built solid phantom with a polyacetal plastic (Delrin®) surface enclosed in a black PVC plastic housing, ensuring the exact positioning of the probe each time [Fig. 1(b)]. Additionally, white reference spectra were recorded using contact measurements on a diffuse polytetrafluoroethylene plastic white reference tile (WS-2, Top Sensor Systems, Eerbeek, The Netherlands) with reflectivity higher than 98% in the 400 to 900-nm range. In-house designed algorithms and software were developed for the data recording and the analysis using LabView (National Instruments, Austin, Texas), and Matlab (Mathworks Incorporated, Natick, Massachusetts), respectively.

2.4 Protocol and Spectral Recordings

Prior to the measurements, the probe was sterilized using the Sterrad™ process.^{10,11} Diffuse reflectance spectroscopy recordings were performed in relation to the following five surgical phases: before aortic cross-clamping (baseline); after aortic cross-clamping and cardioplegic infusion (postcardioplegic infusion); before the release of the aortic cross-clamp (prereperfusion); after the release of the aortic cross-clamp (postreperfusion); and after surgery when the ECC is completely phased out (postCABG) (Fig. 2). During every phase, data were recorded during 10 s for each of the six different locations, three proximal and three distal sites in relation to the left anterior descending coronary artery stenosis (Fig. 3). However, when the stenosis was situated too close to the aortic root, proximal measurements were not possible, and as a consequence, only distal recordings were performed. Anatomical markers were used to ensure a similar measurement site for each DRS recording in the different phases. During the recording of spectra, the probe was held in contact with the myocardial tissue by the surgeon at the predefined

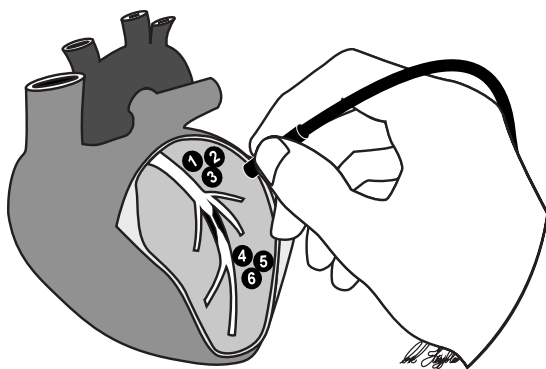


Fig. 3 The measurement sites on the heart. Sites 1, 2, and 3 are proximal to the stenosis, and sites 4, 5, and 6 are distal to the stenosis. Actual sites for each patient were determined by the surgeon using anatomical markers for identification.

sites. Spectra were recorded with an integration time of 200 ms. As reference measurements for each case, three DRS recordings of 10 s each were performed immediately after the last patient measurement, before leaving the operating theater, using the custom built solid phantom. To calibrate the system, three consecutive measurements over 10 s, were recorded using the white reference tile, as well as three intensity reference measurements on the solid phantom on a separate occasion. For all measurements, spectra were recorded in channels 2 to 5 of the spectrometer, where an increasing number corresponds to an increased fiber separation distance [Fig. 1(a)]. Simultaneously, spectra of the light source were recorded in channel 1 through the bifurcated fiber.

2.5 Data Analysis

To eliminate any influences of temporal variations in the light source intensity and color, each recorded tissue spectra (M_{tissue}) were normalized with simultaneously recorded spectra from the light source ($M_{\text{ls,tissue}}$) and were time-averaged over 10 s, forming a single spectrum ($\langle M_{\text{tissue}}/M_{\text{ls,tissue}} \rangle$). The intensity reference measurements (M_{intref}) were likewise normalized by the light source ($M_{\text{ls,intref}}$) and time-averaged to a single spectrum ($\langle M_{\text{intref}}/M_{\text{ls,intref}} \rangle$). The obtained spectrum was finally normalized by white reflectance tile spectra normalized with the corresponding light source spectra ($\langle M'_{\text{whiteref}}/M'_{\text{ls,whiteref}} \rangle$). Note that the prime notation is used to indicate that the intensity reference recordings during tissue measurements and those during white reference tile recordings were made on different occasions. The complete normalization procedure is summarized in Eq. (1), where $M_{\text{tissue,norm}}$ represents the spectra subjected to the analysis of the myocardial tissue oxygenation:

$$M_{\text{tissue,norm}} = \left\langle \frac{M_{\text{tissue}}}{M_{\text{ls,tissue}}} \right\rangle \cdot \frac{1}{\left\langle \frac{M_{\text{intref}}}{M_{\text{ls,intref}}} \right\rangle} \cdot \frac{\left\langle \frac{M'_{\text{intref}}}{M'_{\text{ls,intref}}} \right\rangle}{\left\langle \frac{M'_{\text{whiteref}}}{M'_{\text{ls,whiteref}}} \right\rangle}. \quad (1)$$

The light transport in tissue (T) was modeled according to Jacques, Bargo, and Engelking,⁹ as Eq. (2):

$$T(\mu'_s, \mu_a) = K \cdot \exp[-(\mu_a \cdot L)], \quad (2)$$

where

$$K = a + b \cdot \mu'_s + c \cdot \mu'_s{}^2,$$

$$L = d + e \cdot \mu'_s + f \cdot \mu'_s{}^2. \quad (3)$$

This modified Beer-Lambert model takes into account both light absorption and scattering. Our measurement system was calibrated (coefficients a to f) against a liquid optical phantom grid, with well-defined optical parameters, using Vasolipid (B. Braun Melsungen AG, Melsungen, Germany) as a scatterer, Coloris Ink (Stefan Kupietz GmbH and CoKG, Oldenburg, Germany) as an absorber, and distilled water as a dilutant. The anisotropy (g -value) for the vasolipid was set to 0.7 based on previous studies.^{12,13} The liquid optical

phantom grid was made using seven scattering coefficient values: $\mu_s = [20, 30, 40, 50, 60, 80, 100]_{\lambda=632.8 \text{ nm}} \text{ cm}^{-1}$, and eight absorption coefficient values: $\mu_a = [0.1, 0.2, 0.4, 0.8, 1.6, 3.2, 9.6, 28.8]_{\lambda=632.8 \text{ nm}} \text{ cm}^{-1}$. For each combination of μ_s and μ_a , the diffuse reflectance spectra from the liquid optical phantoms (M_{phantom}), recorded during 10 sec, were normalized similar to $M_{\text{tissue, norm}}$, obtaining $M_{\text{phantom, norm}}$. The probe-specific fitting parameters a to f in Eqs. (3) were estimated by nonlinear curve fitting, utilizing the Levenberg-Marquardt algorithm and $M_{\text{phantom, norm}} = T(\mu'_s, \mu_a)$.

The major chromophores present in heart tissue are oxygenized and deoxygenized hemoglobin and myoglobin (HbO_2 , Hb , MbO_2 , and Mb , respectively), fat (lipid), and water (H_2O). Due to the similarity of hemoglobin and myoglobin absorption spectra,⁷ only the sum of the tissue fractions of the chromophores ($f_{\text{Hb+Mb}}$) was assessed in the spectral fitting described next, using the spectra of hemoglobin. Absorption values for the hemoglobin derivatives have been compiled from data in Tables 8.1 and 8.2 in Zijlstra, Buursma, and van Assendelft,¹⁴ averaging data where overlapping data were found in the two tables. Data were further interpolated around 710 nm to minimize the influence of an irregularity in the tabulated data. The absorption coefficient of fat constituted values provided by Prahl¹⁵ originating from the study presented by van Veen et al.¹⁶ Data for the absorption coefficient of water were taken from the compilation made by Prahl from data presented by Segelstein.¹⁷ The reduced scattering coefficient spectra and the total absorption spectra of heart tissue were hence modeled as Eqs. (4) and (5):

$$\mu'_{s, \text{heart}}(\lambda) = \alpha \cdot \frac{\lambda^{-\beta}}{700^{-\beta}} = \alpha \cdot \left(\frac{\lambda}{700}\right)^{-\beta}, \quad (4)$$

$$\mu_{a, \text{heart}}(\lambda) = f_{\text{Hb+Mb}} \cdot [S \cdot \mu_{a, \text{HbO}_2}(\lambda) + (1 - S) \cdot \mu_{a, \text{Hb}}(\lambda)] + f_{\text{water}} \cdot \mu_{a, \text{H}_2\text{O}}(\lambda) + f_{\text{lipid}} \cdot \mu_{a, \text{lipid}}(\lambda), \quad (5)$$

where α and β are fitting parameters relating to light scattering, $f_{\text{Hb+Mb}}$ is the fraction of hemoglobin and myoglobin, S the tissue oxygenation, f_{water} the fraction of water, and f_{lipid} the fraction of fat. The fraction of water was assumed to be 75% in human heart tissue.⁹ The scattering expression in Eq. (4) is modified from Ref. 9 by the normalization with $1/700^{-\beta}$. The new normalization will make β independent of the absolute level of μ'_s . Thus α governs the level and β the wavelength dependence of μ'_s , something we found that improved the fitting procedure.

A recorded normalized spectrum $M_{\text{tissue, norm}}$ was fitted using the light transport model in Eqs. (2) and (3) with parameters a to f established from calibrating the probe as described previously. The μ_a and μ'_s in Eqs. (2) and (3) are further modeled by Eqs. (4) and (5). The remaining unknown parameters in Eqs. (4) and (5) were determined in two steps using the Levenberg-Marquardt algorithm on selected wavelength intervals. In the first step, the scattering properties α and β were determined for $700 < \lambda < 800 \text{ nm}$ using Eqs. (2) and the first half of Eq. (3). In this wavelength range, the influence from absorption is small. Hence, we assumed $\mu_a = 0$. In the second step, the estimated α and β were used for estimating

$f_{\text{Hb+Mb}}$, S , and f_{lipid} for $530 < \lambda < 585 \text{ nm}$. In this wavelength range, the spectral shapes for oxygenized and deoxygenized Hb+Mb differ in a prominent characteristic way, thereby optimizing the estimation of S . The goodness of fit was calculated for $510 < \lambda < 800 \text{ nm}$ using the Pearson product-moment correlation coefficient R^2 . The choice of the upper limit was to allow for some margin against influences from the surgical head lamp, appearing as peaks around 820 nm; the lower limit was chosen close to the range where the estimation of $f_{\text{Hb+Mb}}$, S , and f_{lipid} was carried out.

To study the temporal change in tissue oxygenation, four comparisons were made between the averages of the measurements in the different surgical phases, postcardioplegic infusion versus baseline; prereperfusion versus postcardioplegic infusion; postreperfusion versus prereperfusion; and postreperfusion versus baseline. When comparing changes in tissue oxygenation, we arbitrarily chose a 5% cutoff value as an indication for increased or decreased oxygenation.

2.6 Data Exclusion and Statistical Analysis

Data from four patients were excluded before analysis, one due to compromised sterility of the probe (patient 3), one due to a broken detection fiber (6), and two where the heart was heavily embedded in fatty tissue, as noted by the surgeon, (5 and 14), giving no signature of hemoglobin in the recorded spectra. The remaining ten patients were included in the final analysis. For five patients, the stenosis was placed low enough to facilitate proximal measurements. The recorded intensity in the receiving fiber with the shortest distance from the source fiber (230 μm) displayed acceptable signal-to-noise ratio (SNR) in the wavelength range 510 to 600 nm for varying concentrations of blood in the sampling volume. For the larger fiber separations, the recorded intensity in this wavelength range was close to the dark current level. Random variations in the dark current, as a function of wavelength, may then cause nonlinear effects for low signal levels. Therefore, numerical data are further presented only for the fiber with the shortest separation distance (230 μm). Myocardial tissue motion occasionally caused probe-tissue contact problems, resulting in nonphysiological intensity variations. Therefore, spectra were discarded if showing an intensity variation, at 640 nm, of more than 30% from the median intensity of the measurement to exclude spectra recorded without surface contact (Fig. 4). At this wavelength, physiological variations in blood volume and tissue oxygenation influence the recorded intensity only to a minor extent, but large fluctuations were found and could be attributed to movement.

Statistical analysis was carried out using Statistica 6.1 (Statsoft Incorporated, Tulsa, Oklahoma). Data were checked for normality using the Lilliefors normality test, and homogeneity of variances between groups were compared using the F-test. The Wilcoxon's matched pairs test was used for comparing groups, where a p -value less than 0.05 was considered significant. The measurements recorded postCABG were not evaluated statistically due to the exclusion criteria leaving too few measurements. For the same reason the proximal measurements were left without statistical analysis.

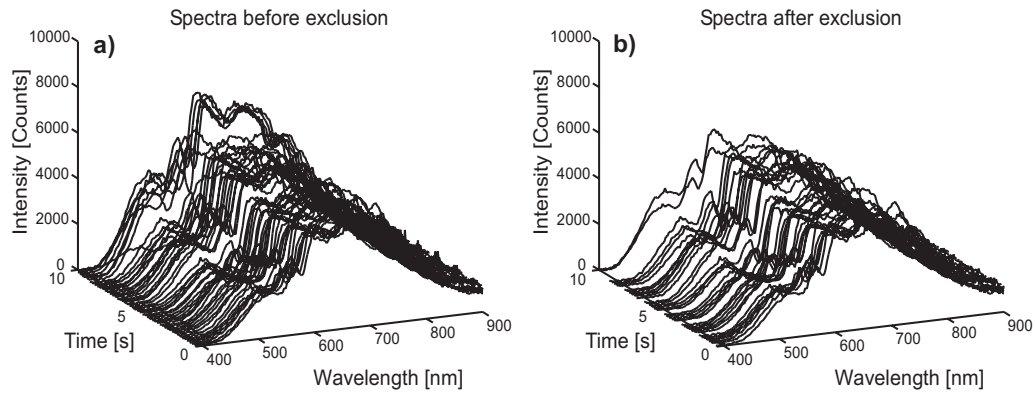


Fig. 4 Diffuse reflectance spectra recorded distal to the stenosis for case 2 during baseline measurements: (a) before and (b) after exclusion of spectra with nonphysiological variations in intensity due to probe-tissue contact problems.

3 Results

The raw spectra from a typical 10-s recording are presented in Fig. 4(a), before and Fig. 4(b) after exclusion of spectra due to probe-tissue contact problems. On average, 9 out of 51 spectra recorded during the 10-s measurements were excluded. The normalized spectrum $M_{\text{tissue, norm}}$ corresponding to data in Fig. 4, and the light transport model $T(\mu'_s, \mu_a)$, are shown in Fig. 5(a); $R^2=0.99$ indicates a good model fit. For some recordings, the light transport model showed a systematic deviation from measured data, as represented by Fig. 5(b); $R^2=0.90$. In these cases, the model overestimated the intensity for wavelengths near $\lambda=510$ nm and near $\lambda=620$ nm. The average R^2 for the distal recordings was 0.96, ranging from 0.86 to 0.99.

The estimated tissue optical properties covered a large range. For the distal recordings: $\mu_a \in [2.0, 21.7] \text{ cm}^{-1}$ and $\mu'_s \in [4.2, 13.0] \text{ cm}^{-1}$ for the wavelength range $\lambda \in [530, 585] \text{ nm}$, and $\mu_a \in [0.1, 0.3] \text{ cm}^{-1}$ and $\mu'_s \in [3.8, 11.0] \text{ cm}^{-1}$ for the wavelength range $\lambda \in [700, 800] \text{ nm}$. The fraction of hemoglobin and myoglobin was in the range $f_{\text{Hb+Mb}} \in [1.0, 7.5]\%$. The wavelength-dependent slope parameter β in Eq. (4) was in the range $\beta \in [0.00, 0.81] \text{ cm}^{-1}$ with nine out of 40 individual values for

the surgical phases, excluding the postCABG phase, being above 0.5. It should be noted that β was limited to positive values, although for some recordings the intensity increased with λ in the β wavelength fitting range ($\lambda \in [700, 800] \text{ nm}$). The results of the β parameter were similar for spectra recorded with fibers having longer source-detector distances compared with the fiber closest to the source used in the data analysis.

Results of the tissue oxygenation are summarized in Tables 1 and 2 for all the cases. For the data recorded proximal to the stenosis, the mean (standard deviation) tissue oxygenation changed from 48 (16)% at baseline to 76 (10)% postcardioplegic infusion, 58 (17)% postreperfusion, and 62 (8)% postCABG (Table 1). The distal data displayed a tissue oxygenation of 55 (9)% at baseline, 68 (23)% postcardioplegic infusion, 58 (23)% prereperfusion, 70 (14)% postreperfusion, and 68 (12)% postCABG (Table 2). Statistical analysis of distal data showed that the variance differed between the surgical phases ($F=7.2$, prereperfusion versus baseline, $p < 0.005$). Tissue oxygenation was significantly higher postcardioplegic infusion and postreperfusion than at baseline ($p < 0.05$), and borderline significantly higher postreperfusion than prereperfusion ($p < 0.06$). Individual comparisons of distal data

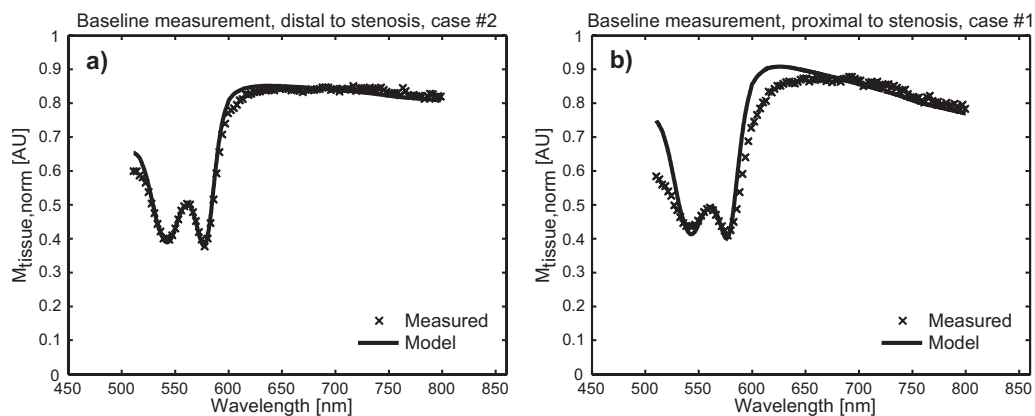


Fig. 5 (a) Normalized tissue spectrum $M_{\text{tissue, norm}}$ [Eq. (1); x-marks] and the fitted spectra using the light transport model $T(\mu'_s, \mu_a)$ [Eq. (2); solid line] with good fit, $R^2=0.99$. (b) Normalized tissue spectrum $M_{\text{tissue, norm}}$ [Eq. (1); x-marks] and the fitted spectra using the light transport model $T(\mu'_s, \mu_a)$ [Eq. (2); solid line] with poor fit, $R^2=0.90$.

Table 1 Tissue oxygenation (percent) for measurements proximal to the stenosis.

Case	Baseline	Postcardioplegic infusion	Postreperfusion	PostCABG
1	62.5	87.0	68.9	68.2
2	57.2	62.5	50.7	—
11	31.5	69.8	45.8	69.4
12	58.5	77.7	81.3	56.7
13	28.8	84.1	41.6	54.0
Mean	47.7	76.2	57.7	62.1
SD	16.2	10.1	16.8	7.8

showed that tissue oxygenation increased during aortic clamping versus baseline in 7 out of 10 cases [Fig. 6(a)]. Tissue oxygenation decreased in 6 out of 10 cases during cardiac arrest [Fig. 6(b)]. Tissue oxygenation increased in 7 out of 10 cases after reperfusion [Fig. 6(c)]. Finally, tissue oxygenation increased in 8 out of 10 cases postreperfusion versus baseline [Fig. 6(d)]. For the proximal measurements, 5 out of 5 cases showed increased tissue oxygenation during aortic clamping and cardioplegic infusion [Fig. 7(a)], and 4 out of 5 cases increased comparing postreperfusion versus baseline [Fig. 7(b)]. The comparisons of the different phases are summarized in Table 3.

4 Discussion

We have presented a method for estimating the oxygenation of heart tissue using a calibrated probe with source-detector distances less than 1 mm. The light transport algorithm proposed by Jacques, Bargo, and Engelking⁹ fits a model in terms of light scattering and absorption (μ'_s and μ_a) to a measured spectrum. We have shown good agreement between the model and the measured spectra (average $R^2=0.96$). The used method has proved to work satisfactorily in the operating theater during bypass surgery, despite the complex measurement situation.

The ability to calibrate the probe in absolute units of μ'_s and μ_a using the light transport model has provided us with estimates, not only of the absorption values for the major chromophores included in the tissue model, but also for the scattering properties of the tissue. Another approach using the second derivative of the spectrum can diminish the influence of the scattering effects when calculating fractional saturation.⁶ However, the model used in this study not only gives the tissue saturation, but also the concentration of the chromophores and level of scattering. This is of paramount importance when modeling the tissue and its contents, but foremost it enables comparisons between individuals despite varying tissue optical properties. This comparison has not been previously possible, since variations in the optical parameters result in differences in photon path lengths and influence the measurement readings.¹⁸ The estimated values for the optical parameters have been found conformant to the findings in pig hearts by Gandjbakhche et al.¹⁹ (μ_a of about 8 cm^{-1} and $\mu'_s=12\text{ cm}^{-1}$).

Table 2 Tissue oxygenation (percent) for measurements distal to the stenosis. The mean SD values of 68.1 and 70.1 for postcardioplegic infusion and postreperfusion are $p<0.05$ versus baseline.

Case	Baseline	Postcardioplegic infusion	Prereperfusion	Postreperfusion	PostCABG
1	48.0	41.1	56.4	82.9	80.7
2	59.0	34.4	83.7	64.9	—
4	48.5	75.5	51.7	62.3	—
7	53.4	36.0	24.0	38.1	—
8	63.4	89.4	67.0	79.0	—
9	62.0	87.5	62.3	74.0	—
10	57.3	71.7	21.9	67.9	—
11	37.2	70.0	88.4	79.3	52.7
12	50.8	83.4	81.1	83.5	73.5
13	65.4	92.2	46.1	69.5	63.2
Mean	54.5	68.1*	58.3	70.1*	67.5
SD	8.6	22.6	23.2	13.5	12.2

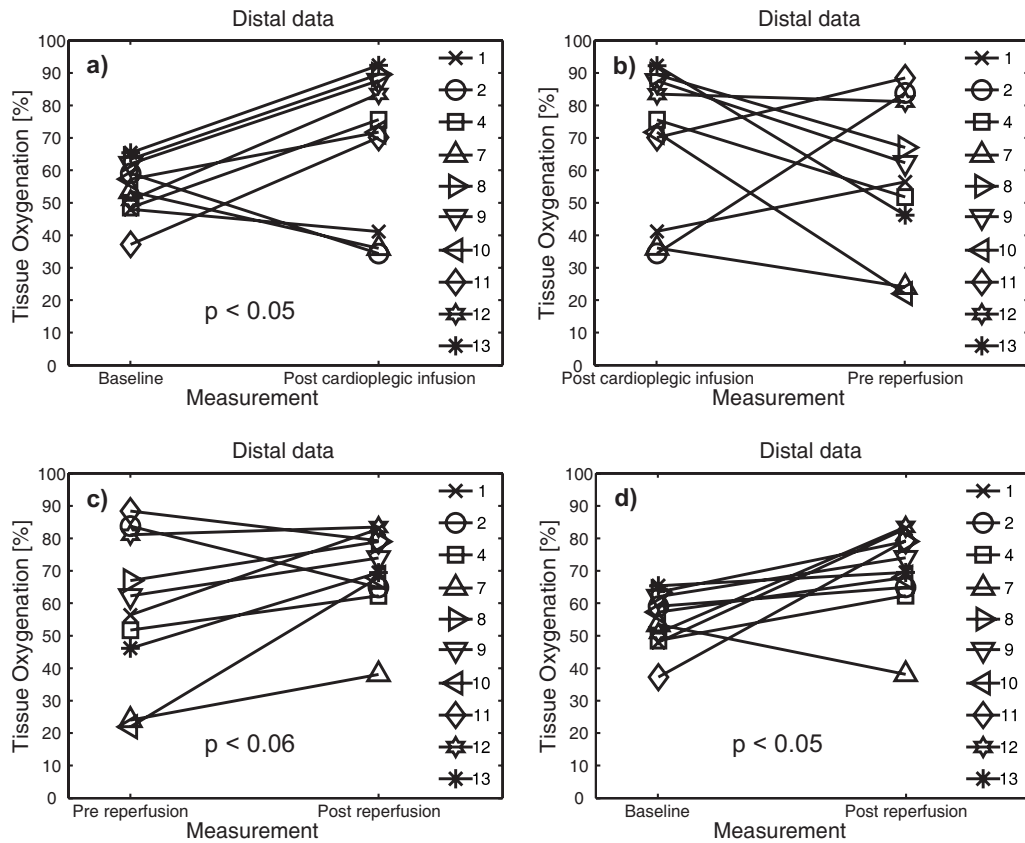


Fig. 6 Tissue oxygenation for the distal measurements comparing different phases in the surgical procedure.

The probe used in the study was designed to enable different sampling volumes; however, the intensity was generally insufficient for longer fiber separations giving unacceptable SNR. The use of a handheld surface probe has not been optimal in achieving stable measurement recordings without data due to motion artifacts. Another study by Perko and Bay-Nielsen²⁰ showed that despite the use of a stabilizing plate with a rough surface, it is still difficult to eliminate such artifacts. However, this study was designed to compare recordings proximal and distal to the stenosis, and therefore a handheld probe was used despite the inherent drawback. Nevertheless, an intramuscular probe would diminish the move-

ment artifacts, and it would also avoid fatty tissue that might surround the heart muscle. At the same time, an intramuscular probe can induce bleeding at the insertion site, which could affect the measurements, something that has been avoided with a surface probe.

During bypass surgery, the tissue oxygenation at the distal sites increased for a majority of the cases when comparing baseline and postcardioplegic infusion. These findings are compatible with previous studies,⁵ which state that myoglobin oxygenation is stable at a level of 91 to 92% during normal cardiac workloads, and only releases oxygen to the mitochon-

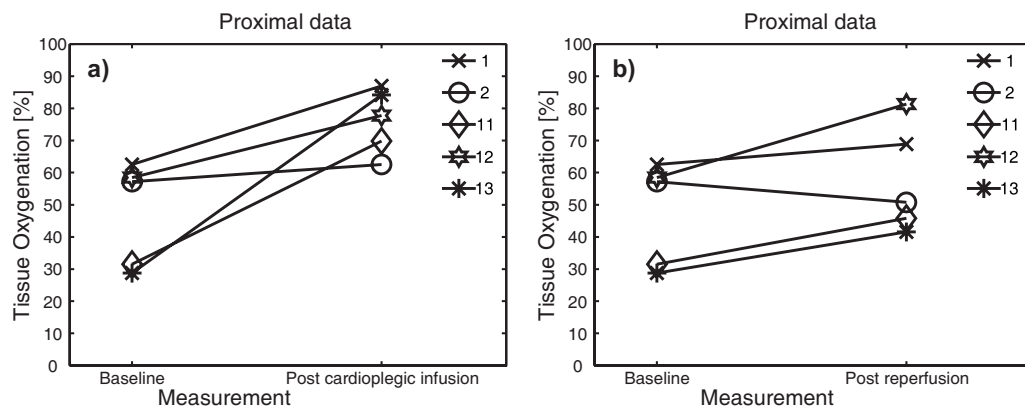


Fig. 7 Tissue oxygenation for the proximal measurements comparing different phases in the surgical procedure.

Table 3 Tissue oxygenation trends during different surgical phases: column 1, postcardioplegic infusion versus baseline; column 2, prereperfusion versus postcardioplegic infusion; column 3 postreperfusion versus prereperfusion; and column 4 postreperfusion versus baseline measurements. The symbols denote: \uparrow increase $>5\%$, \downarrow decrease $>5\%$, and ± 0 no change (change within $\pm 5\%$) in tissue oxygenation.

Trend	1		2		3		4	
	Proximal	Distal	Proximal	Distal	Proximal	Distal	Proximal	Distal
\uparrow	5/5	7/10	—	3/10	—	7/10	4/5	8/10
± 0	—	—	—	1/10	—	1/10	—	1/10
\downarrow	—	3/10	—	6/10	—	2/10	1/5	1/10

dria at very low pO_2 (<2.5 mm Hg).²¹ The increase in tissue oxygenation during reperfusion is probably attributed to the large amount of oxygenated blood inflow from the heart-lung machine. Comparing cardioplegic infusion measurements with measurements before reperfusion demonstrates that the majority of the cases show a decrease in oxygenation at the distal measurement sites. This decrease in tissue oxygenation indicates that the myocardial tissue consumes the oxygen stored in the myoglobin when there is no inflow of blood to the heart muscle. At the proximal sites, it is in general more difficult to form any conclusions, since there are only five eligible cases. Nevertheless, all of the proximal cases show an increase in tissue oxygenation when comparing baseline measurements with postcardioplegic infusion measurements, as well as 4 out of 5 cases showing an increase when comparing measurements postreperfusion with postCABG measurements. Distal to the stenosis, we observed a tissue oxygenation of 55% at baseline, increasing to 68% PostCABG, which is comparable to the increase from 40% at baseline to 50% after revascularization, as observed by Perko and Bay-Nielsen.²⁰

We chose not to separately include both the myoglobin and hemoglobin in the light transport model, but rather represent these oxygen-dependent chromophores with the hemoglobin absorption spectra due to the resemblance of the two chromophores.⁷ This is a drawback of the current method if there is a need to differentiate between bound oxygen in the myoglobin and the oxygen supply of the blood, which can vary independently.^{6,7} If the volume fraction of red blood cells is higher than 2%, a red shift of the spectra postcardioplegic infusion versus baseline is expected due to the absence of hemoglobin.¹⁹

Investigation of the absorption peak around 575 nm did not show this shift, indicating a lower fraction of blood, or that the method cannot resolve such a small shift in measured spectral peaks. Other influences on the recorded spectra might originate from the presence of cytochromes. However, this influence is expected to be less than 10% on the recorded spectra.⁷ In addition, the contribution from fat and water to the total absorption coefficient of the model fit spectra is also considered to be of minor importance, because of the much lower absorption compared to those of oxyhemoglobin and hemoglobin.

In conclusion, we have presented a method using a calibrated probe, accounting for both scattering and absorbing properties of the tissue, for measuring myocardial tissue oxy-

genation during CABG. The method can be applied to a small and flexible probe for intramuscular measurements to minimize motion effects, and for studying temporal changes in oxygenation during CABG and postoperatively.

Acknowledgments

The authors would like to thank Håkan Rohman and Per Sveider for constructing the fiber optic probe and the solid phantom, Marcus Larsson for discussions on probe calibration theory, and the staff at Linköping Heart Center. The study was financed by grants from the Swedish Research Council (2002-5204 and 2005-3934).

References

1. R. A. Lancey, "Off-pump coronary artery bypass surgery," *Curr. Probl. Surg.* **40**(11), 693–802 (2003).
2. M. G. D. Karlsson, C. Fors, K. Wårdell, and H. Casimir-Ahn, "Myocardial perfusion monitoring during coronary artery bypass using an electrocardiogram-triggered laser Doppler technique," *Med. Biol. Eng. Comput.* **43**(5), 582–588 (2005).
3. M. Misfeld, H. Heinze, H. H. Sievers, and E. G. Kraatz, "Intramyocardial oxygen monitoring in coronary artery bypass surgery," *J. Clin. Monit.* **18**(2), 93–101 (2004).
4. H. R. Figulla, K. H. Leitz, J. Hoffmann, and H. Kreuzer, "A new technique for measuring oxygen saturations of hemoglobin and myoglobin and its application in open heart surgery," *Thorac. Cardiovasc. Surg.* **33**(6), 352–335 (1985).
5. A. E. Arai, C. E. Kasserra, P. R. Territo, A. H. Gandjbakhche, and R. S. Balaban, "Myocardial oxygenation in vivo: optical spectroscopy of cytoplasmic myoglobin and mitochondrial cytochromes," *Am. J. Physiol. Heart Circ. Physiol.* **277**(2), H683–H97 (1999).
6. L. S. L. Arakaki, M. J. Kushmerick, and D. H. Burns, "Myoglobin oxygen saturation measured independently of hemoglobin in scattering media by optical reflectance spectroscopy," *Appl. Spectrosc.* **50**(6), 697–707 (1996).
7. K. A. Schenkman, D. R. Marble, D. H. Burns, and E. O. Feigl, "Optical spectroscopic method for in vivo measurement of cardiac myoglobin oxygen saturation," *Appl. Spectrosc.* **53**(3), 332–338 (1999).
8. W. J. Parsons, J. C. Rembert, R. P. Bauman, J. C. Greenfield, Jr., and C. A. Piantadosi, "Dynamic mechanisms of cardiac oxygenation during brief ischemia and reperfusion," *Am. J. Physiol. Heart Circ. Physiol.* **259**(5 Pt 2), H1477–H1485 (1990).
9. S. L. Jacques, P. R. Bargo, and K. Engelking, "Optical fiber reflectance spectroscopy," see <http://omlc.ogi.edu/news/oct03/saratov/index.htm> (25 April, 2007).
10. P. Jacobs and R. Kowatsch, "Sterrad sterilization system: a new technology for instrument sterilization," *Endosc. Surg. Allied Technol.* **1**(1), 57–58 (1993).
11. J. Okpara-Hofmann, M. Knoll, M. Durr, B. Schmitt, and M. Borneff-Lipp, "Comparison of low-temperature hydrogen peroxide gas plasma sterilization for endoscopes using various Sterrad models," *J. Hosp. Infect.* **59**(4), 280–285 (2005).

12. S. Flock, B. Wilson, and M. Patterson, "The optical-properties of tissues at 630 nm and applications to light dosimetry in vivo," *Med. Phys.* **14**(3), 458 (1987).
13. I. Driver, J. W. Feather, P. R. King, and J. B. Dawson, "The optical-properties of aqueous suspensions of intralipid, a fat emulsion," *Phys. Med. Biol.* **34**(12), 1927–1930 (1989).
14. W. G. Zijlstra, A. Buursma, and O. W. van Assendelft, *Visible and Near Infrared Absorption Spectra of Human and Animal Haemoglobin*, pp. 57–61, VSP BV, Leiden, The Netherlands (2000).
15. S. A. Prahl, "Optical absorption of fat," see <http://omlc.org.edu/spectra/fat/> (07 June, 2007).
16. R. L. P. van Veen, H. J. C. M. Sterenborg, A. Pifferi, A. Torricelli, E. Chikoidze, and R. Cubeddu, "Determination of visible near-IR absorption coefficients of mammalian fat using time- and spatially resolved diffuse reflectance and transmission spectroscopy," *J. Biomed. Opt.*, **10**(5), 054004, 2005.
17. S. A. Prahl, "Optical absorption of water compendium," see <http://omlc.org.edu/spectra/water/abs/index.html> (07 June, 2007).
18. H. Nilsson, M. Larsson, G. E. Nilsson, and T. Stromberg, "Photon pathlength determination based on spatially resolved diffuse reflectance," *J. Biomed. Opt.* **7**(3), 478–485 (2002).
19. A. H. Gandjbakhche, R. F. Bonner, A. E. Arai, and R. S. Balaban, "Visible-light photon migration through myocardium in vivo," *Am. J. Physiol. Heart Circ. Physiol.* **277**(2), H698–H704 (1999).
20. M. J. Perko and H. Bay-Nielsen, "Regional myocardial oxygenation during surgical revascularisation," *Cardiovasc. Surg.* **10**(6), 590–594 (2002).
21. K. A. Schenkman, D. R. Marble, D. H. Burns, and E. O. Feigl, "Myoglobin oxygen dissociation by multiwavelength spectroscopy," *J. Appl. Physiol.* **82**(1), 86–92 (1997).